

Article

Coil High Voltage Spark Plug Boots Insulators Material Selection Using MCDM, Simulation, and Experimental Validation

Javier Martínez-Gómez ^{1,2,*}  and Jaime Eduardo Portilla ¹¹ Universidad Internacional SEK Ecuador, Quito EC170134, Ecuador² Departamento de Teoría de la Señal y Comunicación, (Área de Ingeniería Mecánica) Escuela Politécnica, Universidad de Alcalá, 28805 Alcalá de Henares, Spain

* Correspondence: javier.martinez@uisek.edu.ec

Abstract: The examination and choice of an alternate composite material for the high-voltage circuit of Otto cycle internal combustion engines—more commonly known as gasoline engines—are presented in the research that follows. To do this, multicriteria selection procedures are employed, and the outcomes are validated through the use of thermal character simulation software and standard laboratory tests. Nylon is the recommended material for Coils on Plug (COP) high-voltage insulators. Four of the six multicriteria selection techniques utilized in this study were found to be effective. It was discovered through the virtual simulation process that, even in the same environment with the same edge circumstances, the thermal behavior of the materials differs dramatically because the quadrants exhibit different behavior depending on the material. Given that nylon has a lower elasticity modulus than silicone, it was determined that the dimensions are crucial for the nylon Spark Plug Boot (SPB) to comply with the dielectric isolation process. It must have a minimal clearance in order to be related to the geometry of the spark plug and perform the perfect insulation in this manner.

Keywords: MCDM; material selection; simulation; automotive vehicle; Coils on Plug



Citation: Martínez-Gómez, J.; Portilla, J.E. Coil High Voltage Spark Plug Boots Insulators Material Selection Using MCDM, Simulation, and Experimental Validation. *Processes* **2023**, *11*, 1292. <https://doi.org/10.3390/pr11041292>

Academic Editor: Wen-Jer Chang

Received: 2 March 2023

Revised: 20 March 2023

Accepted: 28 March 2023

Published: 21 April 2023



Copyright: © 2023 by the authors. Licensee MDPI, Basel, Switzerland. This article is an open access article distributed under the terms and conditions of the Creative Commons Attribution (CC BY) license (<https://creativecommons.org/licenses/by/4.0/>).

1. Introduction

One of the most crucial steps in the design process for a product is the choice of materials. The process of choosing materials is one that seeks to find the right materials for manufacturing processes from the perspective of engineering design [1]. Each has special qualities that simultaneously affect the product's performance and quality. Consequently, it is essential to choose the right materials for a specific design. Since material selection is a crucial step in product design, designers must start choosing materials as early as possible in the process in order to save costs, increase product success, and reduce product failure. As a result, the material selection must be performed concurrently with the conceptual design.

The primary goal of the conceptual design phase is to find a solution to a design issue prompted by a set of requirements, needs, and specifications. Exploring sets of options in this situation might help you make better selections regarding the choice of materials.

One of the design tactics used to achieve product efficiency is multicriteria decision-making (MCDM) methods for choosing materials [2]. Each product is unique; thus, each one may need a variety of functionalities that cannot all be satisfied by a single material. A design that makes use of a variety of materials is a workable option for achieving a product's functional needs. According to Ashby et al. [1], the use of different materials in product design results in a product that is more useful, capable of being produced, affordable, and aesthetically pleasing. According to [3], MCDM techniques are based on the comparative analysis of candidate materials. Since they are methods that aid in defining the characteristics of what is sought, a list of candidates must be established in order to ascertain what the main function will be and then choose a single one. The author

of [4] asserts that choosing a suitable material to manufacture a product typically entails a comparative evaluation of a number of criteria and material attributes, which are significant when providing the material as a service. As a result, selecting a material that is suitable requires careful consideration of how different materials compare.

Other engineering applications where MCDM was used can be found in Bitarafan et al.'s [5] "Evaluating construction methods of cold-formed steel structures in reconstructing the areas damaged in natural crises, using the AHP and COPRAS-G methods"; Findik and Turan's [6] "Materials selection for lighter wagon design with a weighted property index method"; Zavadskas, EK, Çaliskan, Kursuncu, Kurbanoglu, and Güven's [7] "Material selection for the tool holder working under hard milling conditions using different decision making methods"; and Çaliskan's [8] "Selection of boron-based tribological hard coatings using multi-criteria decision making methods".

On the other hand, it is important to validate the MCDM results. During the product development phase, the design simulation assists manufacturers in validating and confirming a product's intended usage, as well as its manufacturing capabilities [9]. The term "simulation" is frequently used to refer broadly to computer-aided engineering (CAE) [10]. As this efficient, quick, affordable, and user-friendly design simulation software enables users to deal with new technologies and applications, a number of design simulation approaches have become standard components of product development in several sectors and continue to gain relevance.

Simulation models are collections of mathematical equations that depict how a system reacts in an interesting physical area. The difficulty of mathematics varies by application and design stage and is dependent on the data's accessibility [11].

Typically, basic representations of the system are used in the early stages of development to validate the interaction between various physical features at the concept level while using analytical assumptions. Application-specific models are used for validation and refinement in the late stages of development, which are typically quite complicated. Aspects such as structural behavior, acoustics, system dynamics, shock resistance, heat and flow analysis, stress analysis, fuel efficiency, the development of controllers, and much more [12] can be covered by these applications.

In Anderson and Coughlan's paper [13] addressing liquid film flows over solid surfaces and in Boutchel et al.'s study [14] employing wind tunnels to optimize real-world rain scenarios, simulation examples for automobile parts can be found. Gaylard and Duncan also investigated the rear glass and body side vehicle soiling by road sprays in [15]. Roettger et al. investigated the effects of contamination caused by solid particle adherence in [16]. A scale cargo ship was also used in an examination by Wu and Cui [17] into how it behaved in pools during swell.

Nevertheless, none of the aforementioned studies combine laboratory simulation and testing with MCDM methodologies to improve the design process and validate the findings. This paper's goal was to carry out an MCDM on a spark plug boot (SPB). A thermal origin simulation was run using the NX Nas-tram Software in the thermal simulation module, following the MCDM selection process. Ultimately, many SPB specimens made with the material chosen and thought to be ideal were subjected to laboratory testing of a thermal and dielectric nature in order to confirm the simulation's findings.

2. Materials and Methods

The piece's functioning, the characteristics of the materials utilized in the study, an explanation of the MCDM, details on how the simulation was carried out, and the thermogravimetry test are all included in the Materials and Methods. Each of them is explained below.

2.1. Piece Performance

Automobile engines are not complete without ignition coils. These are intricate little gadgets, according to Skinner and Lovers [18], that start combustion in an engine. They

supply the stoichiometric air–fuel mixture with high-voltage electric power (34 kV), or a spark, to ignite it.

Independent coils are the name for these gadgets (coil on plug, COP). The high voltage transformer (HVT), which houses the electrical and electronic pieces responsible for producing high voltage, and the high-tension lead (HTL), which transfers energy from the coil to the spark plug, are the two essential components of COP coils. The HTL can be separated from the coil, it should be noted. The spark plug boot circuit is protected from electrical energy leakage by an electrical insulator that covers the HTL (SPB). Due to the operating conditions, the SPB high-voltage insulation experiences technological degradation, which results in failures such as excessive slack in the boot in the sector that covers the top part of the spark plug or fractures in the material. The end result of this degradation is an electrical energy leak, which results in an incomplete or nonexistent combustion of the stoichiometric mixture in the cylinder where the degradation occurs. As a result, failures such as engine power losses of about 25%, excessive fuel consumption because of compensations managed by the multi point fuel injection system (MPFI), and high pollutant emissions result. These factors necessitate replacing the insulating SPB. The full COP coil, which consists of the SPB and the HVT coil together, rather than the spare part, cannot be found on the Ecuadorian market. However, purchasing the entire COP coil anytime there is a malfunction that just affects the SPB is an unnecessary expense that has negative effects on the economy and the environment (carbon footprint). Hence, being able to independently locate the SPB would be perfect [18].

2.2. Materials

The selection of materials was made by creating a list of seven polymeric materials, which were then assessed using the preliminary criteria listed below:

- Possessing the dielectric, thermal, chemical, mechanical, and other properties required to carry out the specified function.
- Being widely accessible;
- Having a reasonable price.

For Rao [19], choosing the right material is not a simple task, since, in engineering, all or almost all the aspects that involve the action of a material must be taken into account. That is, to build an electrical insulator, more criteria must be taken into account than for dielectric strength, which is why seven criteria within the group of technical criteria have been used along with one economic criterion. Table 1 shows the selected materials and their properties. It is constructed to display the candidate materials and the evaluation criteria in a matrix. As seen in Table 1, the criteria are given the letter C, whereas the materials are given the letter M. Just the first six criteria will be taken into account because Criteria 7 and 8, which relate to chemical properties, have a similar weight across all materials. High-density polyethylene (HDPE), low-density polyethylene (LDPE), polystyrene (PS), polyvinyl chloride (PVC), polyamide 6-nylon (PA6), and a copolymer of ethylene-tetrafluoroethylene (ETFE) and polypropylene (PP) are the materials that are examined. The decision is made in light of the sources [18,20–28] that focus on their attributes. Higher attributes are preferable for all criteria, with the exception of the elasticity module.

2.3. Multicriteria Selection Methods and Weighting Method

VIKOR, PUGH, TOPSIS, PROMETHEE, DOMINIC, and COPRAS are the multicriteria selection procedures that were used. The selection criteria used in the aforementioned approaches must have a weight or quantitative value, which is why the weighting technique known as STATISTICAL VARIATION was used.

Table 1. Selected materials and their properties.

Materials (M)	Dielectric Strength $V \times m$ (C1)	Work Temperature (C2)	Price \$ \times kg (C3)	Coefficient of Thermal Expansion $\times 10^{-6} K^{-1}$ (C4)	Thermal Conductivity $Wm^{-1} K^{-1}$ (C5)	Elasticity Module GPa (C6)	Resistance to Hydrocarbons (C7)	Resistance to Grease and Oils (C8)
Polyethylene HDPE (M1)	22	120	4	100	0.33	0.3	Yes	Yes
Polyethylene LDPE (M2)	22	90	4	100	0.52	1.2	Yes	Yes
Polystyrene (M3)	20	95	4.25	70	0.17	1.65	Yes	Yes
PVC (M4)	14	75	4	75	0.25	4.0	Yes	Yes
Nylon (M5)	25	160	4	95	0.28	3.0	Yes	Yes
Teflon (M6)	25	160	4.5	90	0.24	0.8	Yes	Yes
Polypropylene (M7)	30	120	5	100	0.22	1.5	Yes	Yes

Next, the polymers and why they were chosen are explained.

2.3.1. Statistical Variation Method

It is an objective statistical technique that collects the numerical values for each variable in a predetermined decision matrix and numerically concatenates them until it finds the value that most closely resembles the ideal. The numerically higher criterion is given more weight as a result. The procedures for their application are as follows:

Step 1: Decision matrix construction.

Step 2: Normalization of the decision matrix. In order to determine the relative weights of each criterion, we normalize the decision matrix.

Step 3: Calculation of statistical variation, which could be called the average value of a group of iterations between the values of each criterion.

Step 4: Obtaining weights for each criterion. In this step, the value or attribute that this method assigns to each criterion is granted.

More information about this MCDM can be found in [24,28–45].

2.3.2. VIKOR Method

The MCDM method known as VIKOR was initially created to address issues with choosing criteria and alternatives. The decision-maker seeks a resolution that comes the closest to the ideal, and the alternatives are assessed in accordance with the stated criteria, presuming that compromise is appropriate for conflict resolution. The compromise option that comes the closest to the ideal is identified by VIKOR after ranking the alternatives. The authors of [2,26] provide more details about the VIKOR technique.

2.3.3. PUGH Method

The PUGH technique is employed by Martnez et al. [25] to assess options in a design process by classifying and quantifying criteria, material, methods, traits, etc. They are given a set amount of weight in order to build a scale. This process contains 4 steps:

- Assign point value to each criterion and build the decision matrix. For this, the matrix of the Entropy method is used.
- Give positive (+) or negative (−) values to the characteristics, according to what is sought and build the prioritization matrix. In this matrix, the criteria of the options are compared with the original criteria.
- Numerical values are assigned to this comparison, where better than the original = 1, same as original = 0, and worse than the original = −1
- The third step in obtaining the weighting matrix is to apply,
- Raking. It is the step in which the alternative with the best results must be selected and given a place on the scale, the first position being occupied by the one with the highest value.

More extensive information on method calculations can be found in [25].

2.3.4. TOPSIS Method

By how closely they resemble the perfect answer, preferences are sorted using the TOPSIS approach. The TOPSIS technique uses numerous criteria to select the best option from a limited number of options. The fundamental tenet of the TOPSIS approach is to select the option that is closest to the perfect solution that is positive and farthest from the ideal solution that is ideal. The definition of an ideal solution is a set of ratings or values for every aspect taken into account [12,28]. More extensive information on method calculations can be found in [12].

2.3.5. PROMETHEE II Method

Using a list of alternatives, the PROMETHEE approach creates a series of scales that can be positive, negative, or net depending on the desired characteristics of a particular valuation procedure. The steps are listed in References [26–28]. More extensive information on method calculations can be found in [26].

2.3.6. DOMINIC Method

The Dominic technique is a qualitative way of choosing materials that takes into account the selection criteria's weighted considerations. Matrix calculations are used to choose. The candidate materials, denoted by a letter in the columns, are located between the rows of criteria and weight factors. In [25], the operation procedure is discussed. This research contains further in-depth information on technique computations.

2.3.7. COPRAS Method

The COPRAS approach is a decision-making technique that combines the weights and values of the various criteria. As a result, relative priorities are established depending on the properties desired in a material. These positive and negative priorities are assessed in a fashion that allows for the observation of the performance levels of each material alternative; i.e., their assessment is a percentage. In this approach, it is possible to classify the materials according to how well they perform mathematically [30]. More extensive information on method calculations can be found in [31].

2.3.8. Spearman Correlation Coefficient

Once the findings of the MCDM are acquired, it is necessary to determine whether there is a correlation between them. To do this, a tool such as the Spearman correlation is utilized. The values obtained using this method, according to [29–36], range from -1.0 to 1.0 , going down to 0 , and are interpreted as follows: if they are close to 1.0 , there is a positive correlation; if they are close to -0.1 , there is a negative correlation; and if the value is 0 , there is no connection. That is, in the case of positive correlation, there is an association in which, by increasing the value in a range, the related one also increases; the contrary happens in the case of negative correlation; and, in the case of 0 , it is absent. To do this, the results of the MCDM must be analyzed in pairs, making combinations so that they all come together. More extensive information on method calculations can be found in [2].

2.4. Simulation

The steps to follow to carry out the simulation are insert the 3D geometry of the SPB into the software (CAD), assign material, perform meshing, enter the border conditions, and resolve the simulation.

2.4.1. CAD Model

The first step to carry out the simulation process is to define the geometry of the element to be analyzed. This study seeks to suggest an alternative material with which SPB insulators can be manufactured. In this way, when applying the material, the geometry varies depending on the brand of the engine in which it will work. However, for this study,

the geometry of the SPB insulation of a Suzuki G16B engine incorporated in a Grand Vitara vehicle was taken arbitrarily. The planes are shown below in Figures 1 and 2.

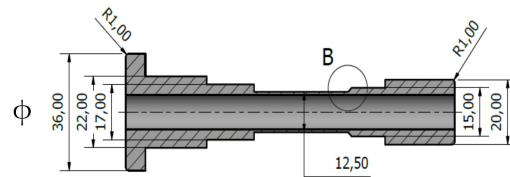


Figure 1. SPB Front and longitudinal view.

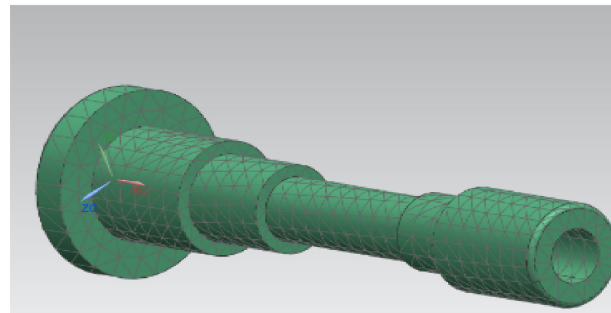


Figure 2. SPB tetrahedral mesh.

2.4.2. Thermal Simulation

The thermal analysis was developed by loading the thermal simulation environment. FEM and SIM, the virtual locations where the simulation in the NX program takes place and where the CAD model of the SPB is loaded, are known as this environment.

The next step is to load the type of material. By selecting the material, all the features are loaded, which are recorded in the software library.

The next step is to create in the 3D CAD model of the SPB, a mesh of finite elements, which must be of tetrahedral type due to the geometry of the insulator. The size of the mesh is calculated by the software, which defined it in 5.82 mm per element, as shown in Figure 2.

The next step is to assign the thermal load W with $Q =$ amount of energy required, $m =$ object mass = 0.04 kg, $C_e =$ specific heat = 1670, $T_f =$ final temperature = 100 °C, $T_i =$ initial temperature = 25 °C, $d =$ material density = 1.14 g/cm³, $v =$ piece column = 36 cm³, $W =$ load = 8.35 W, $e =$ energy = 5010 J, and $t =$ time = 600 s.

2.4.3. Conditions for the Simulation

Border conditions are the set of loads and restrictions that are handled in the form of data to be entered into the software. These are the same in all simulations, except the material and the convection coefficient. Mentioned data are shown in Table 1. The same load value was taken for all the materials. To facilitate the analysis of the results, the piece was divided into six quadrants, as shown in Figure 3.

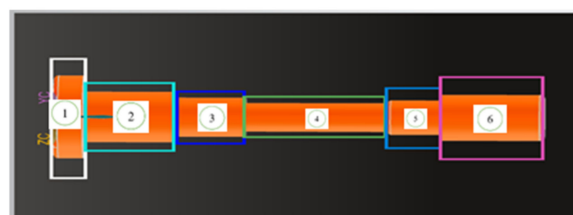


Figure 3. SPB divided into six quadrants.

Simulation border conditions are shown in Table 2. With the purpose of being able to appreciate the changes that the material suffers as a function of time, six images correspond-

ing to simulations made in different phases of time were to be collected, each one being 120 s apart, totaling 10 min, the time in which the engine reaches the working temperature, which is constant from that moment on.

Table 2. Border conditions for simulation.

Material	Load (W)	Temperature °C	Coefficient of Thermal Conductivity 23 °C ($V m^{-1} K^{-1}$)	Thermal Exposure Time from 0 s to 600 s	Computer Time by Simulation (min)
Polyethylene HDPE	30	160	0.3	Yes	10
Polyethylene LDPE	30	160	1.2	Yes	12
Polystyrene	30	160	1.65	Yes	14
PVC	30	160	4.0	Yes	15
Nylon	30	160	3.0	Yes	20
Teflon	30	160	0.8	Yes	17
Polypropylene	30	160	1.5	Yes	21

2.5. Thermogravimetry Test

The testing approach aims to evaluate an SPB prototype constructed with the material's thermal properties with improved outcomes, carried to extreme levels, and beyond those that the material possesses.

For this, an SPB with nylon had to be manufactured, which proved to be the material with the best results. For this, the same geometry of the simulation was used, that of an SPB of a Suzuki G16B engine, mounted on the Grand Vitara 2011 model vehicles, which are some of the ones that present the most electrical insulation problems in the SPB. The method of construction was manual machining. The product is visualized in Figure 1.

Thermogravimetric experimentation was performed in the lab of Ecuador's National Polytechnic School's CIAP Polymer Applied Research Center. According to ASTM D3850-12, "Rapid Thermal Degradation of Solid Electrical Insulating Materials by Thermogravimetric Techniques (TGA)", the test was conducted. Table 3 outlines the test conditions.

Table 3. Test conditions.

Factors	Characteristics/Values
Laboratory:	CIAP/EPN
Norm:	ASTM D3850-12
Equipment:	Thermobalance
Heat rate:	10 °C/min
Gas:	Nitrogen
Gas flow:	50 mL/min
Crucible:	Platinum

3. Results

The results of the simulation in each of the materials, the thermogravimetry test in the selected material, and the results of the MCDM are all included in the materials and techniques. Below is an explanation of each.

3.1. Results of the MCDM

In Table 1, a matrix displaying the potential materials was created. The next stage was to use the multicriteria approaches to choose the material that would technically make the SPB insulators the best. The following criteria have to be precisely taken into consideration in order to use the multicriteria methods: dielectric strength, working temperature, coefficient of thermal expansion, thermal conductivity, modulus of elasticity, resistance to hydrocarbons, resistance to fats and oils, and pricing. Each criterion had to be weighted

after the criteria was established; that is, it had to be determined which criterion was the most crucial in this material. According to Martínez et al. [25], the weighting factors express the relative importance of each criterion. Thus, methods called weighting methods were used to perform this task: statistical variation.

To make the selection by MCDM, it was necessary to determine the values of the weights of each criterion. For this, the values obtained in the statistical variation method were taken as weights, since its results were greater in the dielectric resistance criterion. Because the purpose of this research is to suggest a material to manufacture high-voltage insulators for COP coils, it is important to take into account the values obtained in this particular criterion. For Chérrez-Troya et al. [26], a criterion has greater weight when there is greater diversity in the evaluation of each alternative, meaning that it is important to have several methods to compare results. Next, the results of the statistical variation are explained.

3.1.1. Results of the Statistical Variation Method

First, the normalized matrix was obtained with the maximum and minimum values. The values obtained are grouped in the matrix of Table 4, where the p -values indicate the number of the material accompanied by the value of the criterion they represent.

Table 4. Normalized decision matrix statistical variation method.

p Value	Value of the Criterion	p -Value	Value of the Criterion	p -Value	Value of the Criterion
P11	0.63	P12	0.62	P13	1
P21	0.63	P22	0.39	P23	1
P31	0.7	P32	0.78	P33	0.94
P41	1	P42	1	P43	1
P51	0.56	P52	0.46	P53	0.88
P61	0.56	P62	0.46	P63	0.88
P71	0.46	P72	0.62	P73	0.8

In the next step of the statistical variation method, a value called V_j was obtained, as well as the intermediate values of the statistical variation, as shown in Table 5.

Table 5. Intermediate results of the statistical variation (V).

Numeral of Variation	Value
Vi1	0.0249
Vi2	0.0329
Vi3	0.0049
Vi4	0.0149
Vi5	0.0349
Vi6	0.0869

The next step was obtaining the W weights, which are grouped in Table 6.

Table 6. Weights obtained by the statistical variation method.

w_1	w_2	w_3	w_4	w_5	w_6
0.1229	0.1629	0.0249	0.0739	0.1859	0.4289

3.1.2. Results of the VIKOR Method

In the first place, the decision matrix was made, and it is shown in Table 7, where the values of the criteria and the materials to be studied are grouped.

Table 7. Data to form the VIKOR decision matrix.

Materials (M)	Dielectric Strength MV/m (C1)	Work Temperature °C (C2)	Price \$ × kg (C3)	Coefficient of Thermal Expansion × 10 ⁻⁶ K ⁻¹ (C4)	Thermal Conductivity Wm ⁻¹ K ⁻¹ (C5)	Elasticity Module GPa (C6)
Polyethylene HDPE (M1)	22	120	4	100	0.33	0.3
Polyethylene LDPE (M2)	22	90	4	100	0.52	1.2
Polystyrene (M3)	20	95	4.25	70	0.17	1.65
PVC (M4)	14	75	4	75	0.25	4.0
Nylon (M5)	25	160	4	95	0.28	3.0
Teflon (M6)	25	160	4.5	90	0.24	0.8
Polypropylene (M7)	30	120	5	100	0.22	1.5

The matrix of normalized values is in the next step of the VIKOR method, as shown in Table 8.

Table 8. Normalized matrix VIKOR(Rij).

Code	C1	C2	C3	C4	C5	C6
M1	0.36	0.37	0.34	0.41	0.40	0.053
M2	0.36	0.28	0.34	0.41	0.64	0.21
M3	0.32	0.29	0.37	0.29	0.21	0.29
M4	0.22	0.23	0.34	0.31	0.30	0.70
M5	0.41	0.49	0.39	0.39	0.34	0.52
M6	0.41	0.49	0.39	0.37	0.29	0.14
M7	0.49	0.37	0.43	0.41	0.27	0.26

The next step of the VIKOR method is the standardized VIKOR weight matrix, as shown in Table 9.

Table 9. Standardized VIKOR weight matrix.

Code	C1	C2	C3	C4	C5	C6
M1	0.058	0.009	0.042	0.030	0.075	0.022
M2	0.058	0.007	0.042	0.030	0.119	0.090
M3	0.053	0.007	0.045	0.021	0.039	0.088
M4	0.037	0.005	0.042	0.023	0.057	0.302
M5	0.066	0.012	0.042	0.029	0.064	0.227
M6	0.066	0.012	0.042	0.027	0.055	0.060
M7	0.080	0.009	0.042	0.030	0.050	0.113

The optimal solutions are of two kinds depending on their relevance and covalence, which are called (U_i) and (R_i) here, respectively. These help obtain the grouped values in the matrix of the same name, and they are used for the next step of the method. The best result is the value closest to zero, as the scale goes from 1 to 7 (Table 10).

Table 10. Intermediate VIKOR results.

Optimal Solutions U	Value	Optimal Solutions R	Value	Numerals V _{ij}	Value
U1	0.623	R1	0.429	V1	0.81
U2	0.427	R2	0.325	V2	0.58
U3	0.741	R3	0.329	V3	1.01
U4	0.393	R4	0.163	V4	0.27
U5	0.368	R5	0.128	V5	0.18
U6	0.657	R6	0.371	V6	0.79
U7	0.584	R7	0.290	V7	0.74
U _i Max = 0.741	U _i Min = 0.368	R _i Min = 0.429	R _i Min = 0.128	α =	0.5

It can be observed in the results of the VIKOR method that nylon reached the number-one position, which means that, according to this method, nylon could be effective in the manufacture of SPB. This is due to its low modulus of elasticity, which makes it easy to work with, and its good dielectric strength. For Liu, Liu, and Wu [26], the VIKOR method uses a ranking system in which the best value is the one that approaches 0, and nylon obtained a value closer to 0 than the rest of the materials.

3.1.3. Results of the PUGH Method

First, the standardized decision matrix was used, where the values of the criteria and the materials to be studied were grouped (Table 7). In this matrix, the criteria of the options are compared with the original criteria. This comparison is assigned numerical values. In the end, the values of this assignment are grouped in a matrix represented in Table 11.

Table 11. First step of PUGH weighing matrix.

Criteria	Original Value	W	M1	M2	M3	M4	M5	M6	M7
C1	19.9	0.1629	1.0	1.0	0	−1.0	1.0	1.0	1.0
C2	139.9	0.0249	−1.0	−1.0	−1.0	−1.0	1.0	1.0	−1.0
C3	2.9	0.1229	1.0	1.0	1.0	1.0	1.0	1.0	1.0
C4	249.9	0.0739	−1.0	−1.0	−1.0	−1.0	−1.0	−1.0	−1.0
C5	0.219	0.1859	1.0	1.0	−1.0	1.0	1.0	1.0	0
C6	4.99	0.4289	−1.0	−1.0	−1.0	−1.0	−1.0	−1.0	−1.0

In the second step, the grouped values are obtained in the weighting matrix of Table 12.

Table 12. Second step of PUGH weighing matrix.

	M1	M2	M3	M4	M5	M6	M7
C1	0.163	0.163	0	−0.163	0.163	0.163	0.163
C2	−0.025	−0.025	−0.025	−0.025	0.025	0.025	−0.025
C3	0.123	0.123	0.123	0.123	0.123	0.123	0.123
C4	−0.074	−0.074	−0.074	−0.074	−0.074	−0.074	−0.074
C5	0.186	0.186	0.186	0.186	0.186	0.186	0
C6	−0.429	−0.429	−0.429	−0.429	−0.429	−0.429	−0.429

In this step, values are summed up, obtaining the M values, the same ones that are grouped in the ranking table shown in Table 13. The highest value is that which occupies the first position.

Table 13. PUGH ranking.

Alternative	Ranking
M1	2
M2	2
M3	3
M4	5
M5	1
M6	1
M7	4

In the PUGH method, the results obtained show that both nylon and Teflon are the most suitable materials for manufacturing SPB. According to Martínez et al. [25], within a product design process, the PUGH method is the method that best evaluates the options available in a selection of materials. That is, the mentioned method allows us to clearly handle the variables and their characteristics.

3.1.4. Results of TOPSIS Method

To obtain results from the TOPSIS method, the VIKOR method matrix represented in Table 7 is used. Table 8 of the VIKOR method is used to obtain the decision matrix. Matrix number 8 of the VIKOR method is used for the standardized matrix. The matrix of ideal positive and negative solutions is shown in Table 14.

Table 14. Matrix of ideal positive and negative TOPSIS solutions.

Positive ideal solution	0.3091	3.2250	0.0849	1.4939	0.0245	0.9538
Negative ideal solution	0.0514	2.3299	0.0255	0.8039	0.0093	0.3907

The ranking of solutions to the TOPSIS method is shown in Table 15. The results show that the PVC is the material with the best results of the selection, occupying the first place. This shows that the values of the materials were very tight and that the methods are very sensitive in their application, hence the need to apply several MCDM. For Khorshidi and Hassani [27], the TOPSIS method is able to identify solutions from a finite number of alternatives, of which the best is the one that comes closest to the ideal positive solution. That is, PVC presented results when evaluated with this method, which approached the positive solution proposed by this method.

Table 15. TOPSIS ranking.

Code	Positive Ideal Solution	Ranking
Mat1	0.011919	W7
Mat2	0.029069	W3
Mat3	0.018309	W6
Mat4	0.072649	W1
Mat5	0.055169	W2
Mat6	0.014119	W5
Mat17	0.027729	W6

3.1.5. Results of the PROMETHEE II Method

First, the standard decision matrix was made, where the values of the standardized criteria of the different materials to be studied are grouped (Table 16).

Table 16. Normalized PROMETHEE II matrix.

Code	C1	C2	C3	C4	C5	C6
Mat1	0.359	0.371	0.339	0.411	0.399	0.052
Mat2	0.361	0.281	0.341	0.409	0.641	0.211
Mat3	0.319	0.291	0.371	0.289	0.209	0.289
Mat4	0.219	0.229	0.341	0.309	0.299	0.699
Mat5	0.421	0.489	0.389	0.389	0.339	0.519
Mat6	0.411	0.489	0.389	0.369	0.289	0.139
Mat7	0.489	0.369	0.429	0.409	0.269	0.259

Next, the exceeding net flows are determined, from which the values grouped in Table 17 are obtained.

Table 17. Matrix net flow of exceeding PROMETHEE II.

Code	$\phi C1$	$\phi C2$	$\phi C3$	$\phi C4$	$\phi C5$	$\phi C6$
Mat1	0.22	0.03	0.16	0.10	0.25	0.57
Mat2	0.24	0.04	0.18	0.11	0.28	0.64
Mat3	-0.46	-0.07	-0.35	-0.21	-0.53	-1.21
Mat4	-0.19	-0.03	-0.14	-0.09	-0.22	-0.50
Mat5	0.24	0.04	0.18	0.11	0.28	0.64
Mat6	-0.05	-0.01	-0.04	-0.02	-0.06	-0.143
Mat7	0	0	0	0	0	0

Then the final values of the method are obtained, grouped in Table 18, where higher is better.

Table 18. PROMETHEE II ranking.

Code	Total Net Flow	Ranking
M1	1.333333	2
M2	1.5	1
M3	-2.833333	6
M4	-1.166667	5
M5	1.5	1
M6	-0.333333	4
M7	0	3

The PROMETHEE II method evidenced nylon as the most appropriate material out of the selection. According to Peng and Xia [28], weights play a determining role in the application of this method, which uses compensation purposes to find the solution. The results were validated in the actual field and compared with methods such as TOPSIS, ELECTER, and WAA, showing the effectiveness of its application. That is, as nylon is the best option according to this method; it has a high probability of success, as this method has been applied and contrasted with similar research methods.

3.1.6. Results of the DOMINIC Method

In this step of the method, a weighting matrix is constructed in which criteria are given priority degrees. The values are grouped in the numerical weighting matrix Table 19.

Table 19. DOMINIC numerical weighting matrix.

	M1	M2	M3	M4	M5	M6	M7
C1	5	5	5	7	10	10	10
C2	5	5	1	1	10	10	7
C3	10	10	7	10	5	7	1
C4	10	10	10	10	10	10	10
C5	10	10	5	10	10	10	10
C6	10	7	7	1	10	10	7

Next, the normalized weighting matrix is made, which appears in Table 20.

Table 20. DOMINIC normalized weighting matrix.

	M1	M2	M3	M4	M5	M6	M7
C1	0.815	0.815	0.815	1.141	1.63	1.63	1.63
C2	0.125	0.125	0.025	0.025	0.25	0.25	0.175
C3	1.23	1.23	0.861	1.23	0.615	0.861	0.123
C4	0.74	0.74	0.74	0.74	0.74	0.74	0.74
C5	1.86	1.86	0.93	1.86	1.86	1.86	1.86
C6	4.29	3.003	3.003	0.429	4.29	4.29	3.003

Finally, the ranking of results is calculated, as presented in Table 21.

Table 21. DOMINIC ranking.

Code	Value	Ranking
M1	9.06	3
M2	7.773	4
M3	6.374	6
M4	5.425	7
M5	9.385	2
M6	9.631	1
M7	7.531	5

In the DOMINIC method, nylon occupies the first spot in the ranking, thus being the ideal material among the selection of seven materials. According to Martínez et al. [25], the materials selected by this method have been studied qualitatively, as well as by taking their weight into account. This means that nylon, from the qualitative point of view, is better than its containers to manufacture SPB. Polypropylene occupies the second position in this method since the two materials show the highest values in the criteria in the application process of the DOMINIC method.

3.1.7. Results of the COPRAS Method

For the COPRAS method, the normalized decision matrix was first made, as presented in Table 22.

Table 22. Decision matrix normalized COPRAS.

Code	C1	C2	C3	C4	C5	C6
M1	0.13924051	0.14634146	0.1322314	0.15873016	0.1641791	0.02409639
M2	0.13924051	0.1097561	0.1322314	0.15873016	0.25870647	0.09638554
M3	0.12658228	0.11585366	0.14049587	0.11111111	0.08457711	0.13253012
M4	0.08860759	0.09146341	0.1322314	0.11904762	0.12437811	0.32128514
M5	0.15822785	0.19512195	0.14876033	0.15079365	0.13930348	0.24096386
M6	0.15822785	0.19512195	0.14876033	0.14285714	0.11940299	0.06425703
M7	0.18987342	0.14634146	0.16528926	0.15873016	0.10945274	0.12048193

Next, the standardized weight matrix COPRAS V_{ij} was made, as shown in Table 23.

Table 23. Standardized weight matrix COPRAS Vij.

Code	C1	C2	C3	C4	C5	C6
M1	0.0226962	0.00365854	0.01626446	0.01174603	0.03053731	0.01033735
M2	0.0226962	0.0027439	0.01626446	0.01174603	0.0481194	0.0413494
M3	0.02063291	0.00289634	0.01728099	0.00822222	0.01573134	0.05685542
M4	0.01444304	0.00228659	0.00177649	0.00880952	0.02313433	0.13783133
M5	0.02579114	0.00487805	0.00317231	0.01115873	0.02591045	0.10337349
M6	0.02579114	0.00487805	0.01829752	0.01057143	0.02220896	0.02756627
M7	0.03094937	0.00365854	0.02033058	0.01174603	0.02035821	0.05168675

Then the positive and negative normalized weights, the relative priorities, and the percentage yield are calculated, as shown in Table 24.

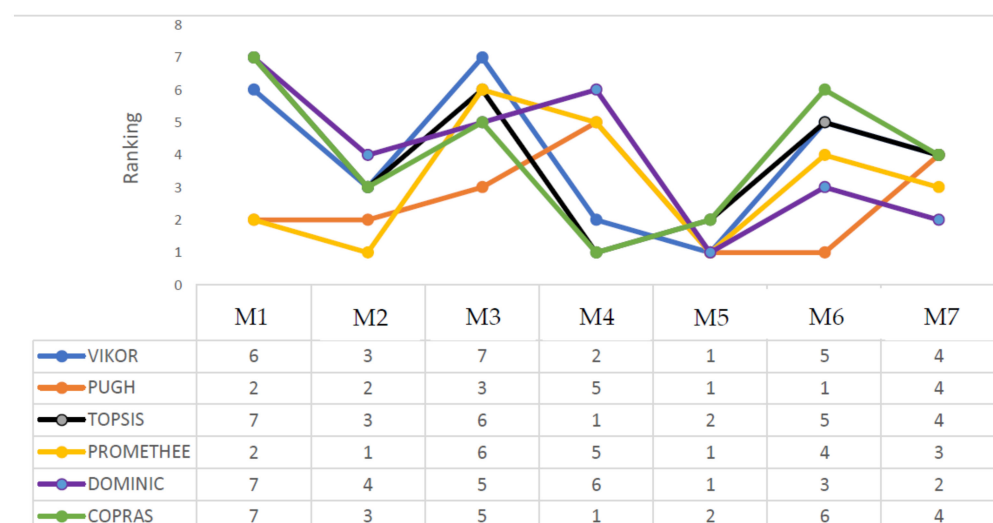
Table 24. Positive and negative normalized weights.

Code	S+	S−	Qi	Values	Ranking
M1	0.0952399	0.01626446	0.100177746	42.9046686	7
M2	0.1429194	0.01626446	0.14785725	63.3251051	3
M3	0.12161923	0.01728099	0.12626662	54.0781529	5
M4	0.18828129	0.00177649	0.23348915	100	1
M5	0.17428417	0.00317231	0.199600569	85.4860147	2
M6	0.10931336	0.01829752	0.113702557	48.6971481	6
M7	0.13872947	0.02033058	0.142679749	61.1076572	4

The COPRAS method determined PVC to be the most suitable material. An interesting point of this method is that nylon holds the second position, which proved to have a higher performance in the majority of results of the other methods. According to Villacreses et al. [2], the level of performance for each alternative is achieved by comparing the priorities of all the alternatives with the most efficient one. That is, the level of performance of PVC evaluated with this method is the highest compared to the performance of other materials, followed by nylon.

3.1.8. Evaluation of the Results for the MCDM Methods

A statistical comparison of the data is shown in Figure 4, where it can be seen that the best material is the one that consistently ranks first overall. Four and three times, respectively, nylon took first and second place.

**Figure 4.** Comparison of MCDM results.

A correlation between the data used is indicated by positive Spearman coefficient results. The presence of correlations above 0.7 suggests a nearly complete correlation with the study variables employed. MCDM techniques are shown in Table 25. The correlation between the VIKOR technique and TOPSIS and COPRAS is 0.92 and 0.85, respectively, indicating a strong correlation. The association between it and the PUGH approach is, however, modest. Correlations with the PUGH technique are often lower than 0.55.

Table 25. Spearman correlation in MCDM results.

	VIKOR	PUGH	TOPSIS	PROMETHEE	DOMINIC
PUGH	0.07	-	-	-	-
TOPSIS	0.92	-0.18	-	-	-
PROMETHEE	0.50	0.54	0.20	-	-
DOMINIC	0.46	0.42	0.46	0.38	-
COPRAS	0.86	-0.30	0.86	0.85	0.28

3.2. Results of Simulation

The simulation results include the thermal simulations of the materials chosen for the study that are explained below in each subsection.

3.2.1. Results of Simulation with Polyethylene LDPE

The results of the simulation with polyethylene LDPE are shown in Figure 5. In Figure 5A, the piece is observed at 0 s of elapsed simulation time—that is to say, at room temperature—where the blue color indicates the absence of a thermal load. In Figure 5B, the piece is shown at 120 s of the simulation, and the work environment of the piece starts to heat up. In this way, a change of color from blue to light blue is observed in Quadrants 1 and 6 of the piece, meaning an upward thermal change in the order of 140 °C, as they are heat-source zones, where there is contact with the spark plug in Quadrant 6 and with the valve cover in Quadrant 1, respectively. Figure 5C shows when 240 s of simulation elapsed. The increase in temperature in Quadrants 1, 4, 5, and 6 becomes noticeable with a color lighter than in the previous figure with a temperature of 154 °C. In Figure 5D, Quadrants 1, 4, and 6 have risen to 156 °C, as indicated by the yellow color and Quadrants 2 and 3 remain in sky blue. In this moment, the phase change of this material begins. It is thus possible that the rest of the insulating and thermal characteristics are affected when exceeding this threshold. In Figure 5E, the temperature reaches 157 °C in Quadrants 1, 4, and 6, while the rest remains with minor variations. In Figure 5F, the engine has already reached the ideal working temperature, programmed in the software, and Quadrants 1 and 6, with an intense red color, are the most affected with 160 °C, while the remaining quadrants remain with minimum elevations, and they do not exceed the barrier of 157 °C and 158 °C.

3.2.2. Results of the Simulation with Polythene HDPE

The results of the simulation with polyethylene HDPE are shown in Figure 6. In Figure 6A, the piece is observed at 0 s of the elapsed time of simulation—that is to say, at room temperature—where the blue color indicates the absence of thermal charge. Figure 6B shows when 120 s has elapsed since the simulation started and the work environment of the piece begins to heat up; thus, a color change from blue to light blue is observed in Quadrants 1, 4, 5, and 6 of the piece, meaning a thermal change of 140 °C. The early appearance of temperature in these quadrants, before the rest of the quadrants, is due to the fact that these areas have contact with the hottest parts of the engine. In Figure 6C, 240 s has elapsed, and the temperature increases in the Quadrants 1, 4, 5, and 6, becoming noticeable with a lighter color than in the previous figure with a temperature of 154 °C. In Figure 6D, Quadrants 1, 4, and 6 have risen to 156 °C, as indicated by the yellow color, and the Quadrants 2 and 3 remain blue and light blue, respectively. In Figure 6E, the temperature reaches 157 °C in Quadrants 1, 4, 5, and 6, while the rest of them remain

with minor variations, except for Quadrant 3, which presents a remarkable increase in the middle section by the order of 154 °C. In Figure 6F, the engine has reached the ideal working temperature programmed in the software, and Quadrants 1, 4, 5, and 6, with an intense red color, are the most affected with 160 °C, while the rest of the quadrants remain with minimum elevations and do not exceed the barrier of 150–154 °C. It should be noted that in this material, at this temperature, there are no changes, such as phase change, conductivity, etc.

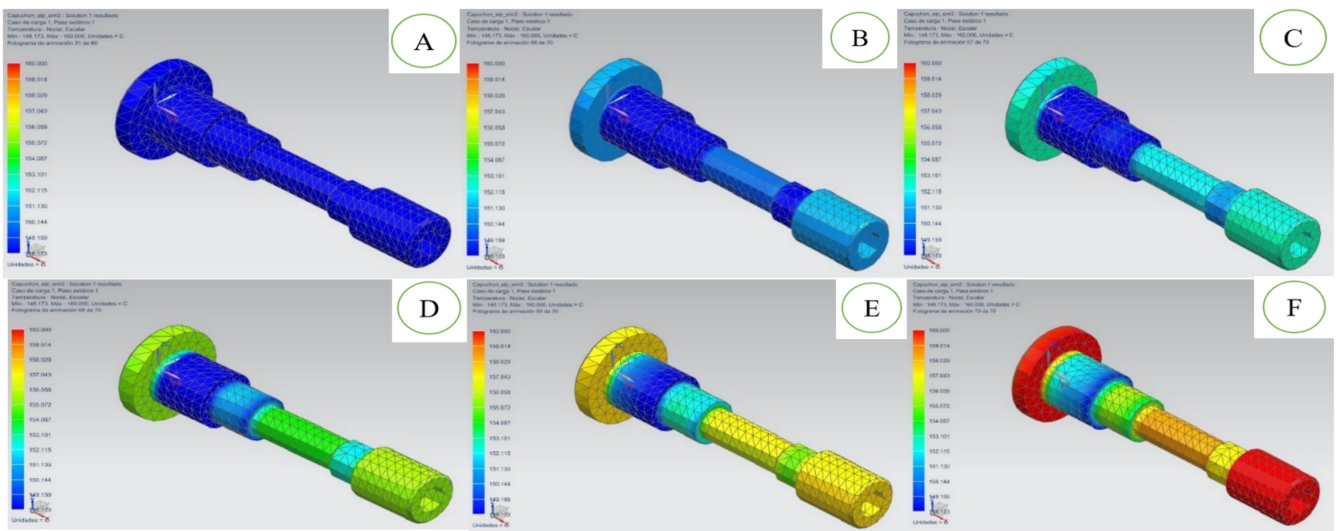


Figure 5. Thermal sequence of polyethylene LDPE from (A–F) related to the time of simulation.

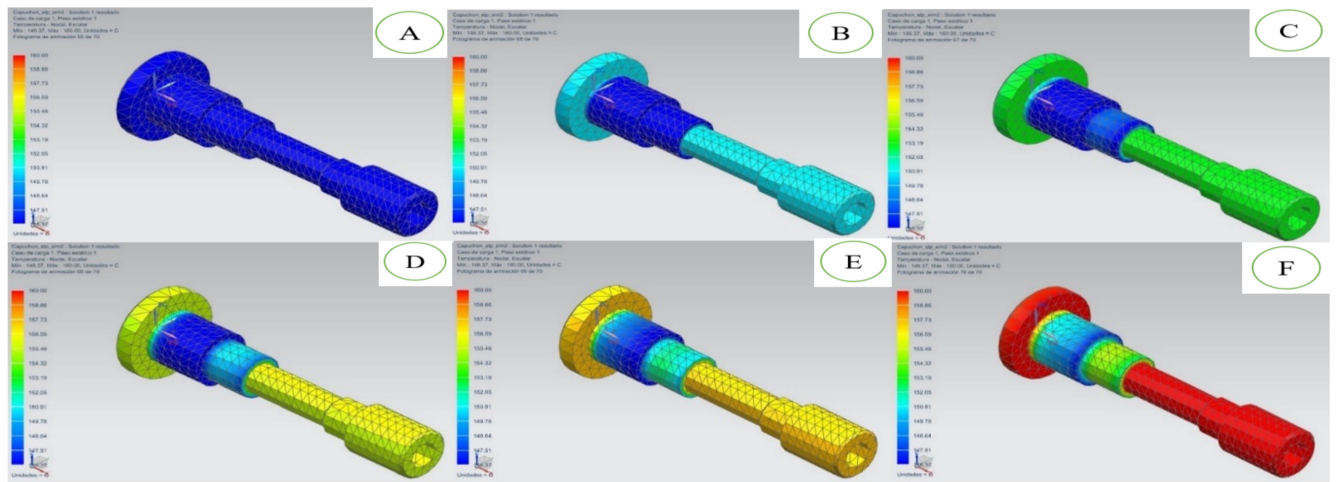


Figure 6. Thermal sequence of polyethylene HDPE from (A–F) related to the time of simulation.

3.2.3. Results of the Simulation with Polystyrene

The results of the simulation with polystyrene are shown in Figure 7. In Figure 7A of the polystyrene, the piece is observed at room temperature, where the blue color indicates the absence of a thermal load. In Figure 7B, 120 s has elapsed since the simulation and the work environment of the piece begins to heat up, thereby showing a change of color from blue to light blue in Quadrants 1, 4, 5, and 6 of the piece, meaning an upward thermal change in the order of 140 °C. Meanwhile, Quadrants 2 and 3 present a thermal increase only at the lower ends. In Figure 7C, 240 s has elapsed, and the increase in temperature in Quadrants 1, 5, and 6 becomes noticeable, with a yellow color, with a temperature of 154 °C; Quadrants 2 and 3 show the same increase in the lower areas; and Quadrant 4 has a green color, indicating a temperature of 154 °C. In Figure 7D, Quadrants 1, 5, and 6 are a

the highest temperature, and the red color shows a temperature of 160 °C, while the same color is presented only in the lower parts of Quadrants 2 and 3. The colors yellow, green, and blue in Quadrants 4, 3, and 2 indicate an increase of up to 157 °C in these areas of the piece. In Figure 7E, with 480 s, the piece turns almost completely orange, indicating a temperature of 158 °C. In Figure 7F, with 600 s, the piece has turned completely red in all its quadrants, reaching a temperature of 160 °C in all the quadrants. It should be noted that, in this material, at this temperature, there are no changes, such as phase change, conductivity, etc.

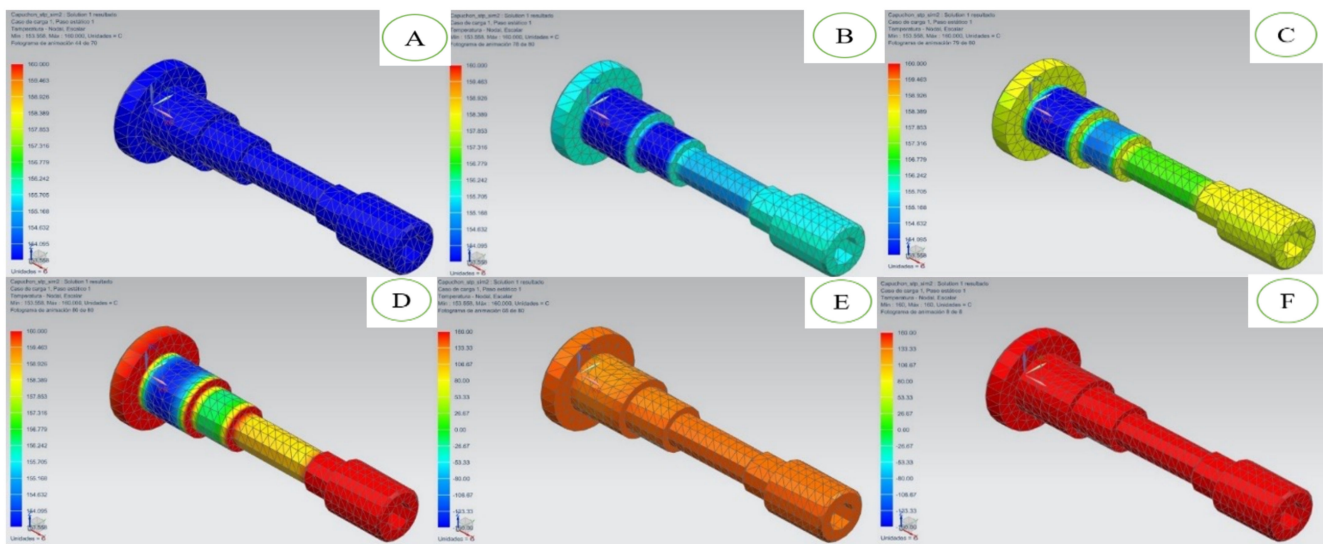


Figure 7. Thermal sequence of polystyrene from (A–F) related to the time of simulation.

3.2.4. Results of Simulation with PVC

The results of the simulation with polystyrene are shown in Figure 8. In Figure 8A of the PVC, the piece is observed at 0 s of the elapsed time of simulation—that is to say, at room temperature—where the blue color indicates the absence of a thermal load. In Figure 8B, 120 s has passed since the simulation, and the piece starts to heat up quickly; thus, a change of color from blue to green is observed in Quadrants 1, 3, 4, and 6, meaning an upward thermal change in the order of 154 °C. The thermal change with PVC was faster due to the characteristics of the material. In Figure 8C, 240 s has elapsed, and the increase in temperature in Quadrants 1, 3, 4, and 6 becomes noticeable, showing a yellow color, with a temperature of 157 °C. Quadrants 2 and 5 remain in blue, with a light blue at the intersection of Quadrants 1 and 2, indicating thermal increase in this area. In Figure 8D, 360 s has elapsed, and the Quadrants 1, 3, 4, and 6 have risen to 157 °C, showing a yellow color. Quadrants 2 and 5 remain blue. In Figure 8E, with 480 s, the temperature reaches 160 °C in Quadrants 1, 4, and 6 only, while Quadrant 3 reaches 157 °C, and the remaining are blue. In Figure 8F, with 600 s elapsed, the Quadrants 2 and 5 and the lower part of Quadrant 3 reach 158 °C, while the rest of the piece reaches 160 °C almost uniformly.

3.2.5. Results of the Simulation with Nylon

The results of the simulation with nylon are shown in Figure 9. In Figure 9A, the piece is observed at 0 s of the elapsed time of simulation—that is to say, at room temperature—where the blue color indicates the absence of a thermal load. In Figure 9B, 120 s has passed since the simulation started, and the work environment of the piece starts to heat up, but in this material, there are hardly any significant changes with thermal increments in the order of 90 °C in Quadrant 2. In Figure 9C, 240 s has elapsed, and only the Quadrants 2, 3, 4, 5, and 6 have reached 120 °C, while Quadrant 1 still has cold blue areas. In Figure 9D, with 360 elapsed seconds, a thermal increase of approximately 3 °C is hardly observed, as compared to the previous figure, and Quadrant 1 remains relatively cold. In Figure 9E,

with 480 s of time, the temperature reaches approximately 157 °C in the quadrants of almost the entire piece, with a slight increase in Quadrant 2, which presents a slight orange pigmentation in a central area, registering around 155 °C. In Figure 9F, corresponding to the simulation with a time of 600 s, the piece remains thermally stable in relation to the previous measurement, showing a notable increase in Quadrant 2, in the order of 157 °C, while in the Quadrant 1, cold areas can still be seen.

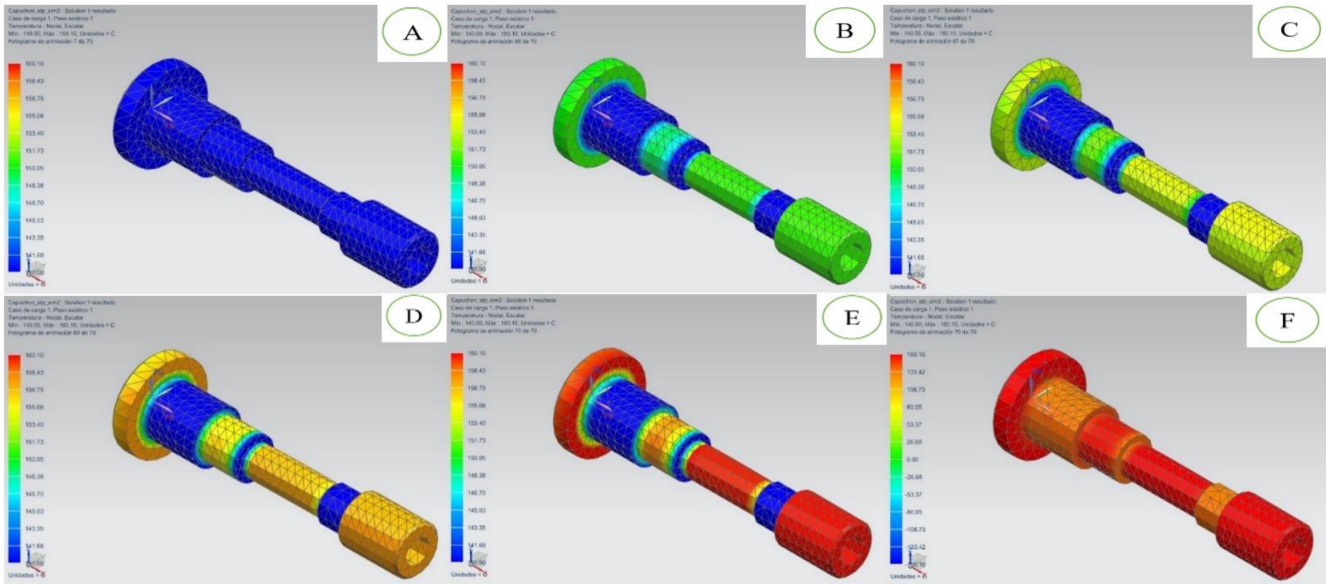


Figure 8. Thermal sequence of PVC from (A–F) related to the time of simulation.

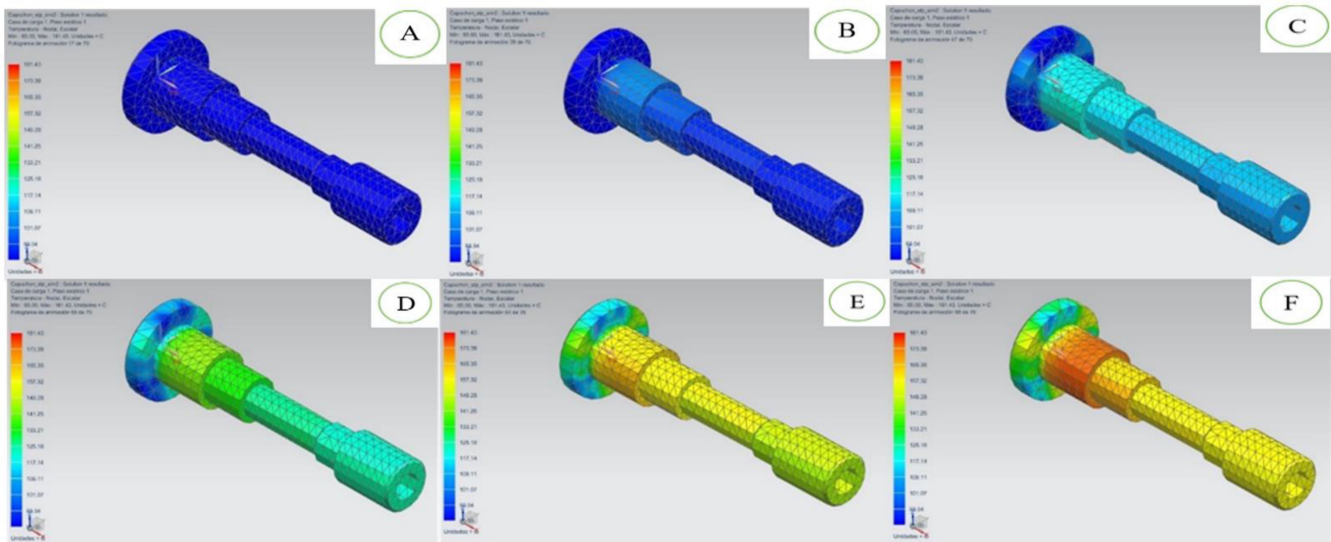


Figure 9. Nylon thermal sequence from (A–F) related to the time of simulation.

3.2.6. Results of the Simulation with Teflon

The results of the simulation with Teflon are shown in Figure 10. In Figure 10A, the piece is observed at 0 s of the elapsed time of simulation—that is to say, at room temperature, where the blue color indicates the absence of a thermal load, action taken in order to notice changes as a function of time. In Figure 10B, 120 s has elapsed since the simulation started, and the work environment of the piece begins to heat up, but in this material, there are hardly any significant changes with thermal increases in the order of 95 °C in Quadrant 2. In Figure 10C, 240 s has elapsed, and only Quadrants 2, 3, 4, 5, and 6 have reached 125 °C, while Quadrant 1 still has cold blue areas. In Figure 10D, with 360 s

elapsed, a thermal increase of approximately 5 °C is hardly observed. Compared to the previous figure, Quadrant 1 remains relatively cold. In Figure 10E, with 480 s of time, the temperature reaches approximately 157 °C in the quadrants of almost the entire piece, with a slight increase in Quadrant 2, which presents a slight orange pigmentation in a central area, registering around 156 °C. In Figure 10F, corresponding to the simulation with a time of 600 s, the piece is kept thermally stable in relation to the previous measurement, showing a notable increase in Quadrant 2, in the order of 157 °C, while in Quadrant 1, cold areas can still be seen.

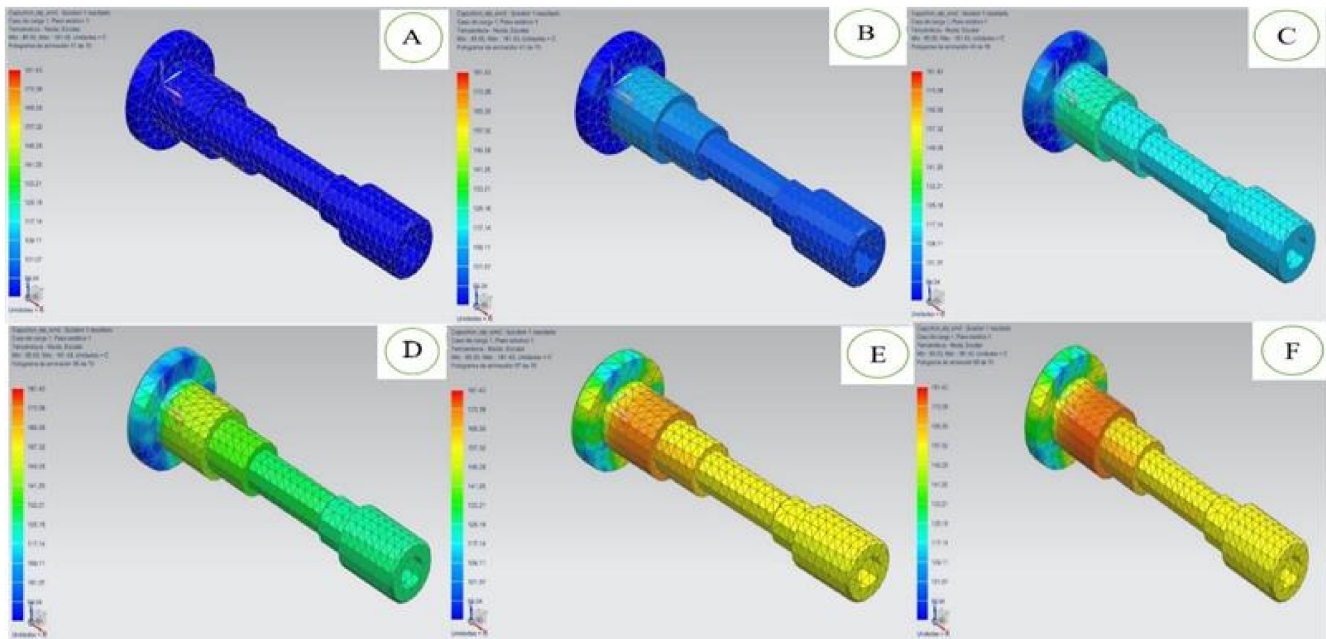


Figure 10. Thermal sequence of Teflon from (A–F) related to the time of simulation.

3.2.7. Results of the Simulation with Polypropylene

The results of the simulation with polypropylene are shown in Figure 11. In Figure 11A, the polypropylene piece is observed at 0 s of the elapsed time of simulation—that is to say, at room temperature—where the blue color indicates the absence of thermal load, action taken in order to notice changes as a function of time. In Figure 11B, 120 s has passed since the simulation started, and the work environment of the piece begins to heat up; thereby, we observed a change of color from blue to light blue in Quadrants 4, 5, and 6 of the piece, meaning an upward heat change of 140 °C, while Quadrants 1, 2, and 3 remained cold. In Figure 11C, 240 s has elapsed, and the increase in temperature in Quadrants 4, 5, and 6 becomes noticeable, showing a green color, indicating a thermal increase of around 154 °C, while, in the remaining quadrants, colors remain cold, with the exception of Quadrant 3. In Figure 11D, Quadrants 4, 5, and 6 have risen to 157 °C, as indicated with the yellow color, and Quadrants 1, 2, and 3 remain in light blue with light green pigments, signaling temperatures of 153 °C. In Figure 11E, with 480 elapsed seconds, the temperature reaches 157 °C in Quadrants 5 and 6 only, while Quadrant 4 remains in degrees. The rest of the quadrants do not exceed 153 °C. In Figure 11F, the engine has reached the ideal working temperature programmed in the software, and Quadrants 5 and 6, with an intense red color, are the most affected, with a temperature of 60 °C, while the rest of the quadrants remain with minimum elevations and do not exceed the barrier of 156 °C. It should be noted that, in this material, at this temperature, there are no changes, such as phase change, conductivity, etc.

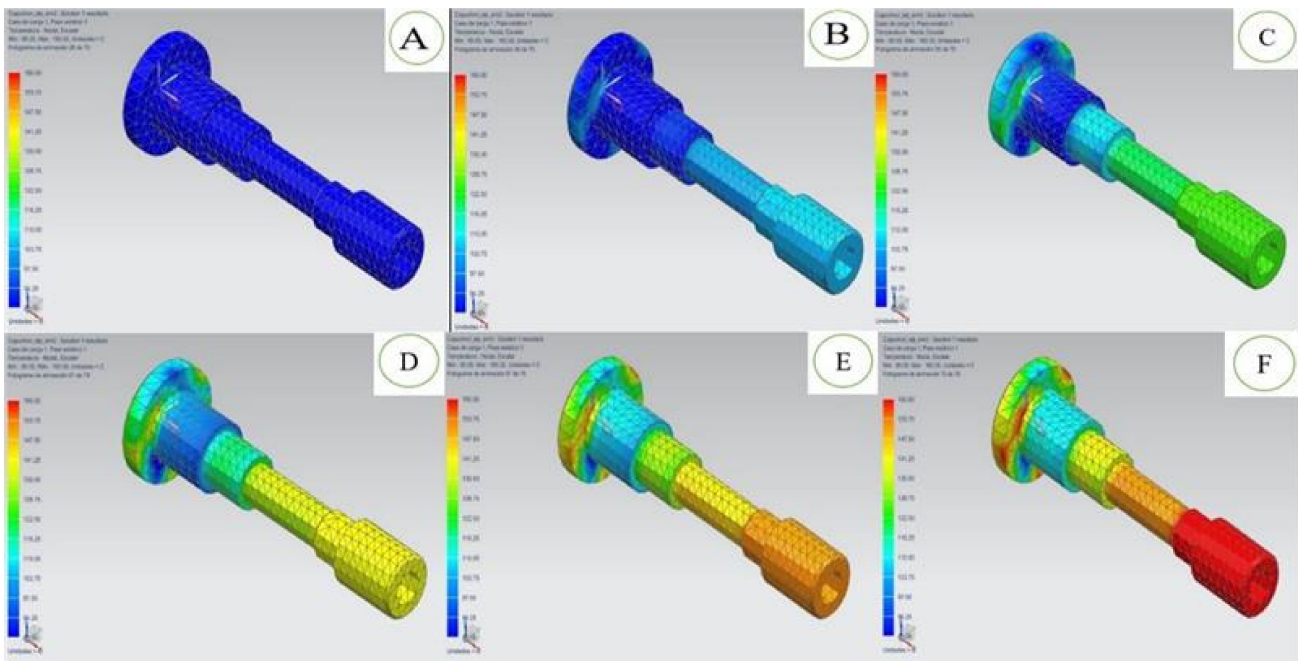


Figure 11. Thermal sequence of polypropylene from (A–F) related to the time of simulation.

3.2.8. Results of the TGA

The results of TGA were carried out on a prototype of SPB made of nylon, which was the best output from the MCDM selection, and virtual simulations of it demonstrated its optimal behavior. Manufacture was performed by manual machining. The simulation’s SPB geometry, which is that of an SPB installed in a Suzuki G16B engine used in Grand Vitara automobiles, served as the basis for the geometry employed. The results of the TGA thermogravimetric test on a prototype made of Polyamide 6 (nylon) can be seen graphically in Figure 12, where the material’s thermal degradation curve begins to approximate 400 °C. This shows that the nylon-made SPB will be able to withstand 140 °C without any problems when it is inserted into the cylinder head of an internal combustion engine.

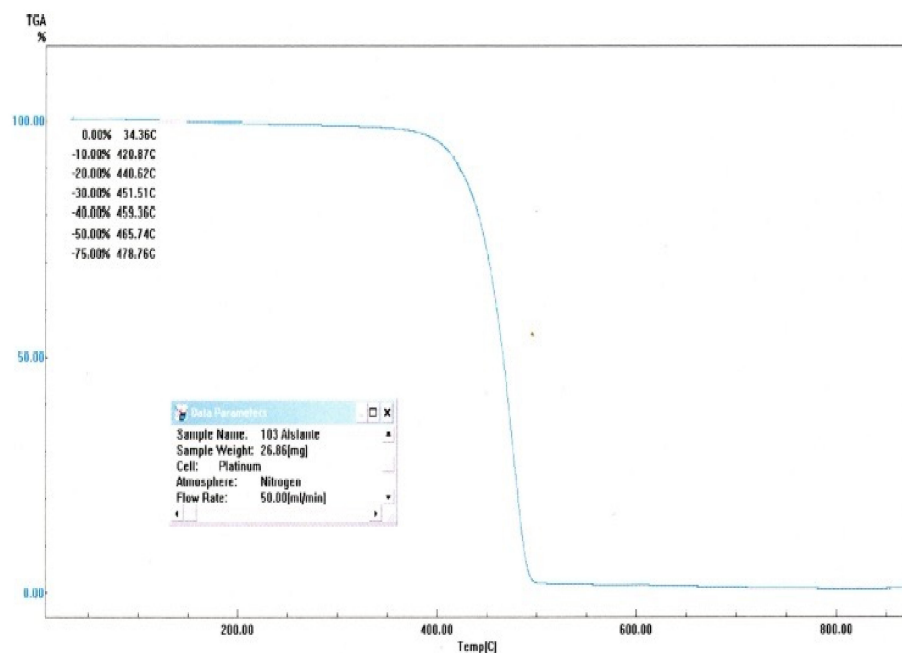


Figure 12. Results of the TGA.

4. Conclusions

The current study was able to choose an alternate composite material to manufacture electrical insulation devices for Otto cycle internal combustion engines' high-voltage circuit. Three selection processes—the use of MCDM, virtual simulations, and experimentation—were used to choose the material. The application of these three techniques allowed for the establishment of concrete limits, while assisting each in validating the others.

It was decided that nylon should be utilized to build high-voltage insulators for COP coils out of the non-traditional materials used to make SPB that were the subject of this study. Four of the six MCDMs employed in this study rank nylon as the first option, while the other two rank it as a second option, an alternative. This indicates that 66.7% of MCDMs rate nylon as the best material for making SPB. PVC would be the second substance on the list. Any MCDM that is employed would benefit from the use of PVC.

It was discovered through the virtual simulation process that, even in the same environment with the identical edge circumstances, the thermal behavior of the materials differs greatly because the quadrants exhibit different behavior depending on the material.

Since that nylon has a lower elasticity modulus than silicone, it was determined that the dimensions are crucial in ensuring that the nylon-built SPB complies with the dielectric isolation method. It must have a minimal clearance in order to be related to the geometry of the spark plug and perform the perfect insulation in this manner. However, in this same way, this disadvantage becomes a strength since it allows the material not to deform when subjected to high temperatures and present less possibility of failure, which does not happen with silicone.

Author Contributions: Conceptualization, J.M.-G. and J.E.P.; methodology, J.M.-G. and J.E.P.; software, J.M.-G. and J.E.P.; validation, J.M.-G. and J.E.P.; formal analysis, J.M.-G. and J.E.P.; investigation, J.M.-G. and J.E.P.; resources, J.M.-G.; data curation, J.M.-G. and J.E.P.; writing—original draft preparation J.M.-G. and J.E.P.; writing—review and editing, J.M.-G. and J.E.P.; visualization, J.M.-G. and J.E.P.; supervision, J.M.-G.; project administration, J.M.-G.; funding acquisition, J.M.-G. All authors have read and agreed to the published version of the manuscript.

Funding: “The APC was funded by University Internacional SEK” and “This research was supported by Universidad Internacional SEK, grant number P121819”.

Data Availability Statement: Not applicable.

Acknowledgments: This study is a component of the Parque de Energías Renovables project P121819, which was started by Universidad Internacional SEK.

Conflicts of Interest: The authors declare no conflict of interest.

References

1. Ashby, M.F.; Cebon, D. Materials selection in mechanical design. *J. Phys. IV* **1993**, *3*, C7-1. [[CrossRef](#)]
2. Villacreses, G.; Gaona, G.; Martínez-Gómez, J.; Jijón, D.J. Wind farms suitability location using geographical information system (GIS), based on multi-criteria decision making (MCDM) methods: The case of continental Ecuador. *Renew. Energy* **2017**, *109*, 275–286. [[CrossRef](#)]
3. Caliskan, H.; Kursuncu, B.; Kurbanglu, C.; Güven, S. Material selection for the tool holder working under hard milling conditions using different multi criteria decision making methods. *Mater. Des.* **2013**, *45*, 473–479. [[CrossRef](#)]
4. Aly, M.F.; Hamza, K.T.; Farag, M.M. A materials selection procedure for sandwiched beams via parametric optimization with applications in automotive industry. *Mater. Des.* **2015**, *56*, 219–226. [[CrossRef](#)]
5. Jahan, A.; Ismail, M.Y.; Sapuan, S.M.; Mustapha, F. Material screening and choosing methods—A review. *Mater. Des.* **2010**, *31*, 696–705. [[CrossRef](#)]
6. Bitarafan, M.; Zolfani, S.H.; Arefi, S.L.; Zavadskas, E.K. Evaluating the construction methods of cold-formed steel structures in reconstructing the areas damaged in natural crises, using the methods AHP and COPRAS-G. *Arch. Civ. Mech. Eng.* **2012**, *12*, 360–367. [[CrossRef](#)]
7. Findik, F.; Turan, K. Materials selection for lighter wagon design with a weighted property index method. *Mater. Des.* **2012**, *37*, 470–477. [[CrossRef](#)]

8. Rangaiah, G.P.; Feng, Z.; Hoadley, A.F. Multi-Objective Optimization Applications in Chemical Process Engineering: Tutorial and Review. *Processes* **2020**, *8*, 508. [[CrossRef](#)]
9. Godoy-Vaca, L.; Almaguer, M.; Martínez-Gómez, J.; Lobato, A.; Palme, M. Analysis of Solar Chimneys in Different Climate Zones-Case of Social Housing in Ecuador. In *IOP Conference Series: Materials Science and Engineering*; No. 7, 072045; IOP Publishing: Bristol, UK, 2019; Volume 245.
10. Castillo, J.P.; Martínez-Gómez, J.; Villacis, S.P.; Riofrio, A.J. Thermal Natural Convection Analysis of Olive Oil in Different Cookware Materials for Induction Stoves. *Int. J. Food Eng.* **2017**, *13*. [[CrossRef](#)]
11. Gomes, L.C.; Miranda, J.; Mergulhão, F.J. Operation of Biofilm Reactors for the Food Industry Using CFD. In *Computational Fluid Dynamics in Food Processing*; CRC Press: Boca Raton, FL, USA, 2018; pp. 561–590.
12. Castillo, J.P.; Martínez, J.; Riofrio, A.J.; Villacis, S.P.; Orozco, M. A Computational fluid dynamic analysis of olive oil in different induction pots. In *Proceedings of the 1st Pan-American Congress on Computational Mechanics—PANACM, Buenos-Aires, Argentina, 27–29 April 2015*; pp. 729–741.
13. Beltrán, R.D.; Martínez-Gómez, J. Analysis of phase change materials (PCM) for building wallboards based on the effect of environment. *J. Build. Eng.* **2019**, *24*, 100726. [[CrossRef](#)]
14. Anderson, A.; Coughlan, B. Liquid film flows over solid surfaces. In *Proceedings of the 6th MIRA International Vehicle Aerodynamics Conference*, Gaydon, UK, 25–26 October 2006; pp. 368–379.
15. Bouchet, J.P.; Delpech, P.; Palier, P. Wind tunnel simulation of road vehicle in driving rain of variable intensity. In *Proceedings of the MIRA Aerodynamics Conference*, Warwick, UK, 13 October 2004.
16. Gaylard, A.P.; Duncan, B. Simulation of rear glass and body side vehicle soiling by road sprays. *SAE Int. J. Passeng. Cars-Mech. Syst.* **2011**, *4*, 184–196. [[CrossRef](#)]
17. Gaylard, A.P.; Kirwan, K.; Lockerby, D.A. Surface contamination of cars: A review. *Proc. Inst. Mech. Eng. Part D J. Automob. Eng.* **2017**, *231*, 1160–1176. [[CrossRef](#)]
18. Wu, Y.S.; Cui, W.C. Advances in the three-dimensional hydroelasticity of ships. *Proc. Inst. Mech. Eng. Part M J. Eng. Marit. Environ.* **2009**, *223*, 331–348. [[CrossRef](#)]
19. Skinner, A.A.; Lovers, H.O. Ignition Coil. U.S. Patent 7,268,655, 25 August 2015.
20. Rao, R.V. A decision making methodology for material selection using an improved compromise ranking method. *Mater. Des.* **2008**, *29*, 1949–1954. [[CrossRef](#)]
21. Aldás, P.S.D.; Constante, J.; Tapia, G.C.; Martínez-Gomez, J. Monohull ship hydrodynamic simulation using CFD. *Int. J. Math. Oper. Res.* **2019**, *15*, 417–433. [[CrossRef](#)]
22. Turner, A. Foamed polystyrene in the marine environment: Sources, additives, transport, behavior, and impacts. *Environ. Sci. Technol.* **2020**, *54*, 10411–10420. [[CrossRef](#)]
23. Xu, S.; Camp, C.H., Jr.; Lee, Y.J. Coherent anti-Stokes Raman scattering microscopy for polymers. *J. Polym. Sci.* **2022**, *60*, 1244–1265. [[CrossRef](#)]
24. Acurio, K.; Chico-Proano, A.; Martínez-Gómez, J.; Ávila, C.F.; Ávila, Á.; Orozco, M. Thermal performance enhancement of organic phase change materials using spent diatomite from the palm oil bleaching process as support. *Constr. Build. Mater.* **2018**, *192*, 633–642. [[CrossRef](#)]
25. Rahim, A.A.; Musa, S.N.; Ramesh, S.; Lim, M.K. A systematic review on material selection methods. *Proc. Inst. Mech. Eng. Part L J. Mater. Des. Appl.* **2020**, *234*, 1032–1059. [[CrossRef](#)]
26. Kabak, Ö.; Ervural, B. Multiple attribute group decision making: A generic conceptual framework and a classification scheme. *Knowl.-Based Syst.* **2017**, *123*, 13–30. [[CrossRef](#)]
27. Chingo, C.; Martínez-Gomez, J. Material selection using multi-criteria decision making methods for geomembranes. *Int. J. Math. Oper. Res.* **2020**, *16*, 24–52. [[CrossRef](#)]
28. Wang, C.N.; Yang, F.C.; Vo, N.T.; Nguyen, V.T.T. Wireless communications for data security: Efficiency assessment of cybersecurity industry—A promising application for UAVs. *Drones* **2022**, *6*, 363. [[CrossRef](#)]
29. Dang, T.T.; Nguyen, N.A.T.; Nguyen, V.T.T.; Dang, L.T.H. A two-stage multi-criteria supplier selection model for sustainable automotive supply chain under uncertainty. *Axioms* **2022**, *11*, 228. [[CrossRef](#)]
30. Liu, H.C.; Liu, L.; Wu, J. Material selection using an interval 2-tuple linguistic VIKOR method considering subjective and objective weights. *Mater. Des.* **2015**, *52*, 158–167. [[CrossRef](#)]
31. Huynh, T.T.; Nguyen, T.V.; Nguyen, Q.M.; Nguyen, T.K. Minimizing warpage for macro-size fused deposition modeling parts. *Comput. Mater. Contin.* **2021**, *68*, 2913–2923.
32. Mousavi-Nasab, S.H.; Sotoudeh-Anvari, A. A new multi-criteria decision making approach for sustainable material selection problem: A critical study on rank reversal problem. *J. Clean. Prod.* **2018**, *182*, 466–484. [[CrossRef](#)]
33. Wang, X.; Zhang, R.; Zhang, K.; Shao, L.; Xu, T.; Shi, X.; Li, D.; Zhang, J.; Xia, Y. Development of a Multi-Criteria Decision-Making Approach for Evaluating the Comprehensive Application of Herbaceous Peony at Low Latitudes. *Int. J. Mol. Sci.* **2022**, *23*, 14342. [[CrossRef](#)]
34. Villacreses, G.; Martinez-Gomez, J.; Jijon, D.; Cordovez, M. Geolocation of photovoltaic farms using Geographic Information Systems (GIS) with Multiple-criteria decision-making (MCDM) methods: Case of the Ecuadorian energy regulation. *Energy Rep.* **2022**, *8*, 3526–3548. [[CrossRef](#)]

35. Nenzhelele, T.; Trimble, J.A.; Swanepoel, J.A.; Kanakana-Katumba, M.G. MCDM Model for Evaluating and Selecting the Optimal Facility Layout Design: A Case Study on Railcar Manufacturing. *Processes* **2023**, *11*, 869. [[CrossRef](#)]
36. Nicolalde, J.F.; Cabrera, M.; Martínez-Gómez, J.; Salazar, R.B.; Reyes, E. Selection of a phase change material for energy storage by multi-criteria decision method regarding the thermal comfort in a vehicle. *J. Energy Storage* **2022**, *51*, 104437. [[CrossRef](#)]
37. Nicolalde, J.F.; Martínez-Gómez, J.; Vallejo, J. Multicriteria Decision Making of a Life Cycle Engineered Rack and Pinion System. *Processes* **2022**, *10*, 957. [[CrossRef](#)]
38. Villacreses, G.; Jijón, D.; Nicolalde, J.F.; Martínez-Gómez, J.; Betancourt, F. Multicriteria Decision Analysis of Suitable Location for Wind and Photovoltaic Power Plants on the Galápagos Islands. *Energies* **2022**, *16*, 29. [[CrossRef](#)]
39. Abdullah, F.M.; Al-Ahmari, A.M.; Anwar, S. An Integrated Fuzzy DEMATEL and Fuzzy TOPSIS Method for Analyzing Smart Manufacturing Technologies. *Processes* **2023**, *11*, 906. [[CrossRef](#)]
40. Nicolalde, J.F.; Cabrera, M.; Martínez-Gómez, J.; Salazar, R.B.; Reyes, E. Selection of a PCM for a Vehicle's Rooftop by Multicriteria Decision Methods and Simulation. *Appl. Sci.* **2021**, *11*, 6359. [[CrossRef](#)]
41. Wang, C.-N.; Thanh, N.V.; Su, C.-C. The Study of a Multicriteria Decision Making Model for Wave Power Plant Location Selection in Vietnam. *Processes* **2019**, *7*, 650. [[CrossRef](#)]
42. Nicolalde, J.F.; Yaselga, J.; Martínez-Gómez, J. Selection of a Sustainable Structural Beam Material for Rural Housing in Latin América by Multicriteria Decision Methods Means. *Appl. Sci.* **2022**, *12*, 1393. [[CrossRef](#)]
43. Godoy-Vaca, L.; Vallejo-Coral, E.C.; Martínez-Gómez, J.; Orozco, M.; Villacreses, G. Predicted medium vote thermal comfort analysis applying energy simulations with phase change materials for very hot-humid climates in social housing in Ecuador. *Sustainability* **2021**, *13*, 1257. [[CrossRef](#)]
44. Uslu, B.; Eren, T.; Gür, Ş.; Özcan, E. Evaluation of the Difficulties in the Internet of Things (IoT) with Multi-Criteria Decision-Making. *Processes* **2019**, *7*, 164. [[CrossRef](#)]
45. Majercikova, Z.; Dibdiakova, K.; Gala, M.; Horvath, D.; Murin, R.; Zoldak, G.; Hatok, J. Different Approaches for the Profiling of Cancer Pathway-Related Genes in Glioblastoma Cells. *Int. J. Mol. Sci.* **2022**, *23*, 10883. [[CrossRef](#)]

Disclaimer/Publisher's Note: The statements, opinions and data contained in all publications are solely those of the individual author(s) and contributor(s) and not of MDPI and/or the editor(s). MDPI and/or the editor(s) disclaim responsibility for any injury to people or property resulting from any ideas, methods, instructions or products referred to in the content.